Molecular Dynamics Simulation of Mechanical Properties of Intercalated GO/C-S-H Nanocomposites

Ding Fan[1,2], Shangtong Yang[2*], Mohamed Saafi[3]

[1] *Shanghai Engineering Research Center of 3D Printing Materials, Shanghai Research Institute of Materials, Shanghai 200437, China*

[2] *Department of Civil and Environmental Engineering, University of Strathclyde, Glasgow, G1 1XJ, United Kingdom.*

[3] *Department of Engineering, Lancaster University, Lancaster, LA1 4YW, United Kingdom.*

ABSTRACT

Graphene oxide (GO) cementitious composites have recently attracted considerable interest due to their improved mechanical properties and durability. However, most research is focused on the macroscale performance of these composites with very little experimental and modelling research on the characterization of their nanoscale behavior. This makes the design of these new GO-cementitious composites challenging. In this paper, we present a novel molecular dynamics (MD) model for GO-cementitious nanocomposites to understand their behavior and predict their mechanical and fracture properties. In this model, different numbers of GO nanoplatelets were inserted into the C-S-H structure and a number of nanoscale mechanical parameters and crack bridging mechanism were obtained. The MD simulation results revealed that the addition of GO sheets increased the tensile and compressive strength of C-S-H by roughly 50% and 100%. The MD simulation results also identified a double-peak phenomenon which is an indication of additional plasticity when the intercalated GO/C-S-H structures are subjected to compressive stress. The fracture simulation results showed that the failure mode of the intercalated GO/C-S-H composites was marked by high energy release. The results of fracture simulations with different notch lengths also indicated that the addition of GO could improve the fracture performance due to a good interfacial connection between the GO and the C-S-H gel.

KEYWORDS: Graphene oxide; Cementitious materials; Molecular dynamics modeling; Nanocomposites; Mechanical properties; Fracture.

* Corresponding author. Tel: +44 141 548 3273. Email: shangtong.yang@strath.ac.uk.

1. INTRODUCTION

There has been a concerted research effort to improve the mechanical properties and durability performance of cementitious composites using a variety of macrofibers[1-5]. Nanomaterials have been extensively used in cementitious nanocomposites to enhance their properties. Amongst these nanomaterials, graphene oxide (GO), is considered to be a potentially good inclusion in cememtitious composites as nano-material. This is because of its distinctive properties including better dispersibility in water due to hydroxyl functional groups, high specific area and high mechanical properties[6]. A considerable amount of research revealed that the addition of GO improved the flexural and compressive strength of GO cementitious composites[7-9]. The literature review also suggested that the large aspect ratio of GO helped improve the overall durability of cement-based materials by reducing permeability and chloride ingress[10].

Calcium silicate hydrates (C-S-H) gels are the main phases of the cement hydration products, which provide the most cohesion and strength of the cement matrix. The C-S-H gels are typically imperfect crystalline with a density of 2.604 g/cm^3 and a chemical formula $(CaO)_{1.7}(SiO_2)(H_2O)_{1.80}$, measured by combining small-angle neutron and X-ray scattering data[11, 12]. Richardson [13] has developed Tobermorite/Jennite (T/J) model and Tobermorite/Calcium Hydroxyl (T/CH) model for interpreting the atomic structure of C-S-H. The T/J model combines the Tobermorite and Jennite domains while the T/CH model contains Tobermorite silicate chains sandwiching calcium hydroxide with Ca/Si ratios higher than 1.0. Pellenq, Kushima, Shahsavari, Van Vliet, Buehler, Yip and Ulm [14] proposed a realistic model for the atomic structure of the C-S-H with a mean Ca/Si value of 1.7, based on the 11Å Tobermorite crystalline structure. To achieve high Ca/Si value in establishing the molecular structure of C-S-H, the long silicate chains were defected according to results from ^{29}Si nuclear magnetic resonance (NMR)[15]. Water molecules were randomly added in the molecular system to achieve a density of 2.6 g/cm^3 for C-S-H. Another C-S-H model was hypothetically formulated for C/S ratio lower than

1.6[16] in which a number of dimeric and pentameric Si-O tetrahedra structures were proposed. In these structures, calcium atoms were coordinated to 6, 7 or 8 oxygen atoms. Meanwhile, the interface between the C-S-H particles plays an important role in the mechanical behavior of C-S-H at the mesoscale. Based on the colloid model[17, 18], Fan and Yang [19] determined the interfacial properties between the unit C-S-H particles/globules via molecular dynamics method. By assuming the maximum packing of C-S-H globules, large-scale simulations of C-S-H at the colloidal level (~15nm) were conducted and the deformation and mechanical property were obtained[20].

When GO sheets are present in the cement matrix, their functional groups enable them to react with the C-S-H gel to produce a strong chemical bond which leads to improved mechanical properties. To better understand the strengthening effect of GO, molecular dynamics (MD) simulations can provide unique insight into the mechanical behavior of GO-cementitious composites by elucidating the main mechanical and chemical interaction mechanisms between the two materials at nanoscale. MD simulations have successfully been used to understand the hydration process of cementitious materials and calculate their deformation, stress, and other molecular properties[21-23]. Such simulations are particularly useful when physical nanoscale experiments are not available. Alkhateb, Al-Ostaz, Cheng and Li [24] was perhaps the first to investigate the microcosmic properties of GO/C-S-H using the MD approach. In their study, COMPASS force field was applied on a unit cell with a layer of GO in the middle of the C-S-H structure. A pull-out test was conducted for calculating the interfacial strength and energy. Fan, Lue and Yang [25] investigated the complete shearing mechanism between GO and C-S-H through MD simulations with ReaxFF force field, and quantitatively derived the full shear stress-strain curve. Hou, Lu, Li, Ma and Li [26] examined the intrinsic interaction between GO and C-S-H and suggested that the functional groups could stabilize the atoms in the C-S-H gel and enhance its mechanical strength at the nanoscale.

Research efforts on understanding the interaction mechanisms between GO and C-S-H and their effect on the nanoscale mechanical properties are rather limited. Amongst the relevant work, Yang, Jia, Hou, Li, Jiang and Zhang [27] found the weakening effect of moisture content on GO reinforced C-S-H composite causing a decrease in failure strength of the structure. Wan and Zhang [28] provided the bond information between GO and C-S-H in details, and Lu, Zhang and Yin [29] presented the structure evolution of the interface between GO and C-S-H at high temperature. However, the fracture properties and failure modes of intercalated GO/C-S-H remain a knowledge gap. Therefore, this paper aims to examine the mechanical properties of GO-cementitious composites, and uncover their fracture behavior and failure modes through MD simulations. In these MD simulations, different numbers of GO sheets were inserted into the C-S-H gel to form intercalated GO/C-S-H structures. The mechanical and fracture properties, and the failure modes of the GO/C-S-H composites were determined, and compared to previous experimental data. Further, the effect of different notch sizes on the mechanical performance of the GO/C-S-H was investigated and the crack bridging mechanism of the GO sheets was elucidated.

2. MODEL CONSTRUCTION

The C-S-H structure used in this study is from Richardson [16]. It is a Tobermorite-based monoclinic structure having 11 Å mean length of silicate chains, 14 Å interlayer spacing and Ca/Si ratio of 0.82. This structure is a good representation of the imperfect crystalline C-S-H (e.g. the coordination of Ca-O) and the existence of intraglobular pores (IGP)[18]. The atomic structure of GO used in this study is based on the Lerf-Klinowski GO model[30]. In addition, the epoxy and hydroxyl functional groups of the GO sheet are randomly distributed[31] to avoid the reduction of energy caused by the agglomeration of the functional groups[32]. Usually, the oxidation of the graphene sheet should range from 4:1 to 2:1 in terms of the C/O ratio[33]. The distribution of oxygen atoms is based on the density functional theory (DFT) analysis[32, 34]. The O-H bond length is found to be 0.98 Å and the angle of C-O-H bond is 107.9°. The attached carbon atom is distorted out of the

plane by 0.37 Å. The hydrogen and oxygen atoms are placed at the same plane perpendicular to the basal plane for simplicity..

The molecular structure of C-S-H and one layer of GO sheet embedded in the C-S-H gel is shown in Figure 1. The chemical formula of the C-S-H is $Ca_4H_2(Si_2O_7)_2Ca4H_2O$ and the lattice parameters are a = 11.35 Å, b = 7.3 Å and c = 21.5 Å and duplicated 4 × 6 × 2 along the x, y, z directions, respectively. The GO sheet was inserted into the inter Calcium layer which is a natural cleavage plane[35] and also the weakest layer in the structure. The simulation box hence has the lattice parameters a = 45.4 Å, b = 43.8 Å, c = 61.46 Å. The C-S-H gel contained one, two and three GO sheets with a C/O ratio of 3.2 and hydroxyl/epoxy ratio 4.5. The GO were placed in the cleavage plane. To examine their effect on the overall performance of the GO/C-S-H composite structures, the GO sheets were adjusted to fit into the size of the C-S-H unit with the period boundary conditions. The C-S-H gel and the GO/C-S-H intercalated structures were then subjected to compressive and tensile stress along the y and z directions.

LAMMPS[36] was used to perform the MD simulations. ReaxFF has been used in C-S-H structures[20, 37], making it reasonable to model the GO-cementitious composites. The timestep was set as 0.25 fs. After energy minimization, the simulation box was relaxed for 500 ps in the isobaric-isothermal ensemble (NPT) and each structure was coupled to zero external pressure in the x, y, z dimensions. The Nose-Hoover thermostat was used to keep the temperature at 300 K, and the Nose-Hoover barostat was used to maintain the pressure at p = 0 Pa. After reaching equilibrium, the system was then subjected to a tensile or compressive stress along the z or y axis with a constant loading rate of 0.08 Å/ps. To obtain the mechanical properties along the z direction, the pressure in the x and y directions was kept at zero; and for determining the mechanical response along the y-direction, the pressure in the x and z directions was also kept at zero.

Figure 2 shows the molecular structure of C-S-H with 2 and 3 sheets of GO. To eliminate the natural separation in the interface between the GO sheets and the C-S-H gel, an extra

relaxation step under compressive pressure was applied along the z-direction before NPT relaxation. To create compression, a strain is added to the entire structure in the z-direction. For the compressive and tensile tests, the starting structure was chosen when the stress started to increase from zero. In this process, it is believed that the separation between the GO sheet and C-S-H can be removed without incurring any additional stress. In this case, the thickness of the interface decreases from 7.9 Å, 17.8 Å and 25.0 Å, to 7.2 Å, 13.5 Å and 20.3 Å for the 1, 2 and 3 GO sheets, respectively. The potential energy and RMSD (root-mean-square deviation) value during the relaxation period of three structures containing GO sheets are shown in Figure 3. The RMSD is defined as follows:

$$RMSD = \sqrt{\frac{\sum_{i=1}^{N_{atoms}}[r_i(t_1)-r_i(t_2)]^2}{N_{atoms}}} \quad (1)$$

where $r_i(t)$ means the position where atom i is at time t and N_{atoms} is the number of atoms being compared. It has shown that both the potential energy and RMSD stop increasing after 350 ps for all structures. It is therefore, in this study, a relaxation period of 350 ps is chosen for all nanocomposite structures. In addition , the relaxation time for the pure C-S-H structure is about 300 ps[38] as well.

To investigate the fracture behavior of the nanocomposites, a notch with a width of 8 Å along y direction and infinite depth along x direction was induced in both C-S-H and C-S-H with 1 non-periodic GO sheet. For both structures in Figure 4, four notches were cut with depths of 5 Å, 10 Å, 15 Å and 20 Å along z direction.

3. RESULTS AND DISCUSSION

3.1. Mechanical properties of GO/C-S-H composites

The stress-strain curves for all GO/C-S-H intercalated structures under tensile stress (y direction) and compressive stress (z direction) are shown in Figure 5. As it can be seen,

the four structures exhibited similar linear stress-strain relationships in the elastic stage with slightly different gradients. The initial tangent modulus of the intercalated GO/C-S-H composites is higher than that of the plain C-S-H gel and appears to increase with increasing the number of the GO sheets. As depicted in Figure 5a, all stress-strain curves are marked by a yielding phase. This yielding phased however is more pronounced in the plain C-S-H. From Figure 5a, one can see a sudden drop of the tensile stress which is followed by a stress yielding stage, and the sudden drop after the first peak indicates the breakage of GO sheet(s). Such a behavior prevents the sudden release of fracture energy when a crack is propagated thereby enhancing the fracture resistance of C-S-H.

As depicted in Figure 5b, the structures exhibited different stress-strain relationships under compressive stress. The addition of GO significantly increased the compressive strength of the C-S-H gel but it seems to have no effect on the compressive initial tangent modulus. The GO also substantially increased the energy absorbed in the C-S-H gel during the loading as reflected by the increase in the areas under the curves. However, when the number of GO is relatively high in a given small space (i.e., 2 and 3 GO layers in the current simulation box), a repaid energy release occurred after the peak stress which led to the appearance of second stress peak which corresponds to the maximum compressive stress. The residual stresses observed in the stress-strain curves are the same for all structures. However, the presence of GO sheets can significantly increase the strength and the work/energy required to fail the GO/C-S-H structure.

The MD simulation results suggest that GO increases the plasticity of the GO/C-S-H composite in compression. As shown in Figure 5b, the compressive stress-strain responses of the intercalated GO/C-S-H composites are marked by two peaks compared to one peak for the plain C-S-H. For one GO sheet, the maximum stress occurred at the first peak; while for higher GO sheets, the maximum stress occurred at the second peak. The second stress peak becomes clearer and more noticeable when the number of GO is increased.

188 This two-peak phenomenon demonstrates the enhancement of plasticity of the C-S-H as a
189 result of GO.

190 The molecular morphology of the C-S-H and GO/C-S-H structures with different numbers
191 of GO sheets under tension at typical stages are shown in Figure 6. This figure shows the
192 effect of the number of the GO sheets on the failure mode of the C-S-H at nanoscale. As
193 depicted, the failure of the structures in tension occurs where the silicate chain is broken.
194 Some local atoms are relocated when the GO sheets start to break just after the maximum
195 stress. Figure 6(a_0 – a_{yii}) shows that under tension, the cracking of the pure C-S-H structure
196 tend to occur close to the left boundary of the simulation box, whereas, the failure of the
197 intercalated GO/C-S-H composites seems to be due to the failure of the GO sheets as
198 shown in Figure 6(b_{yii}, c_{yii} and d_{yii}). The MD simulations elucidate the interaction between
199 the GO sheet and the C-S-H gel. The C-C bonds in the GO sheets, typically much stronger
200 than the chemical bonds in the C-S-H gel, are transferred to the C-S-H which results in
201 stronger composites.

202 As illustrated in Figure 7, under compressive stress, the intercalated GO/C-S-H composites,
203 showed a time delay-difference from the re-configuration of the C-S-H structure to the
204 breakage of the GO sheets, which is probably the reason for the two-peak phenomenon in
205 the stress-strain curves as discussed above. This means that the C-S-H gel will likely break
206 first and after 50 ps, be followed by the failure of the GO sheets. Because of this, when
207 more GO sheets are added, the second peak becomes more pronounced. According to the
208 hydrogen bond networks between GO sheets[39] and structure of C-S-H[40], for
209 multilayer GO sheets, the interlayer molecular interaction between the GO sheets[34]
210 provide a weaker connection than the intrinsic interaction within the C-S-H gel and thus
211 yields no improvement in the initial tangent modulus of the GO/C-S-H gels. The
212 interactive (hydrogen) bonding system between GO sheets are illustrated in Figure 8.

213 The mechanical properties of the composites were determined from the stress-strain curves.
214 The addition of GO increased the maximum tensile strength of the intercalated GO/C-S-H

composites by 19%, 34% and 45% for 1, 2 and 3 GO sheets, respectively. The addition of GO also increased the tensile initial tangent modulus by 13%, 28% and 38% for 1, 2 and 3 GO sheets, respectively. The GO significantly improved the compressive strength of the C-S-H gel and it was increased by 16%, 51% and 96% for 1, 2 and 3 GO sheets, respectively. The improvement of the mechanical properties of the intercalated GO/C-S-H composites in our study can be attributed to strong inherent bond between the GO and the C-S-H gel[26], as shown in Figure 9.

3.2. Validation of the MD results

To date, there are no experimental data on nanoscale mechanical properties of GO/C-S-H composites. This makes the direct verification of the MD results impossible. In this paper, we compare the mechanical properties of nanoscale C-S-H from the simulated MD results and the experiments from literatures which will show the robustness of the MD method and partially verify the model. Given the scarce nanoscale experimental data on GO/C-S-H composites, we believe this procedure can provide reasonable validation strategy and bring in added confidence of using MD method for cementitious nanocomposites research.

The experimental results on Young's modulus and hardness of C-S-H with different Ca/Si ratio are obtained from literature[41]. The hardness achieved from the nanoindentation test is related to the mean pressure sustained beneath the indenter before permanent deformation. The Young's modulus and hardness from experiments are in the range of 93.3 to 115.8 GPa and 12.4 GPa to 13.8 GPa, respectively, for Ca/Si ratio of 0.78 to 0.88. The simulated results are 114.06 and 12.58 for Young's modulus and compressive strength respectively, for Ca/Si equal to 0.82. It can be found that the simulated results are in a reasonable agreement with those of nanoindentation test for modulus and strength of C-S-H. It may be noted that the Young's modulus of C-S-H phases (from Qomi, Krakowiak, Bauchy, Stewart, Shahsavari, Jagannathan, Brommer, Baronnet, Buehler and Yip [41]) is about ten times bigger than the nano-indentation results of cement paste[42].

This is due to the 'size effect' or upscalling effect of cement paste since the nano-indentation test works on larger scales than current MD simulation.

3.3. Fracture properties of the notched molecular structures

The fracture behavior and properties of materials are typically obtained by testing notched samples under tension. The notch enables stress concentration and damage to be localised in one area to accurately measure the fracture properties of materials. In this paper, we investigate the fracture properties of C-S-H and GO/C-S-H structures, and the bridging mechanisms of GO using MD simulations. Like experimental fracture tests, notches of depths 5 Å, 10 Å, 15 Å and 20 Å were cut in the structure of the C-S-H gel and the GO/C-S-H composites containing one GO sheet. In the MD simulations, the GO sheet bridges the notch at different depths under tensile stress. The tensile force was applied directly to the C-S-H molecular structure which is then transferred to the GO sheet through the interfacial bond. The stress-strain curves for all the structures are presented in Figure 10. For notch depths of 5 Å and 10 Å, the bridging effect of GO is somewhat negligible. For deeper notch depths, GO seems to enhance the plasticity of the C-S-H gel. However, the MD simulations did not show any increase in the fracture strength of the C-S-H composites when the GO sheet is present. Further studies are required to confirm these findings.

The morphology of the C-S-H structure with and without one GO sheet equipped with notches of 15 Å and 20 Å under tension at three stages are shown in Figure 11. These three stages are equilibrium, maximum tensile stress and failure. It can be seen that the notch size affects the fracture behavior of the composites. The bridging effect provided by the GO sheet (Figure 10) inhibits failure of the parallel silica chains, thus preventing the C-S-H from cracking.

The fracture strength and the fracture energy values obtained from the fracture results with different notch size are displayed in Figure 12. The tensile strength is decreased as the notch depth increases, similar trend for the fracture energy. This is in line with the common

understanding that notch or impecfection would degrade the strength and fracture resistance of materials. However, it is interesting to find out one GO sheet has little effect (even slightly weakening possibly due to the interface atomic configuration) on the fracture strength and energy of notched C-S-H for notch size up to 15 Å. For notch size over 15 Å, both fracture strength and fracture energy start to increase.

We also conducted a pull-out test on the GO using MD simulations to determine its bond strength. In these simulations, the GO sheet was anchored into the two completely separate parts of C-S-H structure through which the tensile load was applied. The change in the molecular structure of the GO/C-S-H is shown in Figure 13(a)-(c). As shown, GO sustained the pull-out force through the interfacial bond which was calculated about 0.8 GPa (Figure 13d). Figure 13d shows the stress-strain response of the GO/C-S-H structure during the pull-out test. As shown, the GO sheet can partially restore the integrity of a severely cracked C-S-H gel since otherwise there will be no bridging stress.

4. CONCLUSIONS

In this paper, we have conducted molecular dynamics simulations to gain a fundamental understanding of the behavior of intercalated GO/C-S-H composites and determine their performance in terms of mechanical and fracture properties and crack bridging mechanisms. The MD simulation results revealed that the addition of GO could increase the tensile strength by 16% to 45% and the compressive strength by 19% to 96% with one to three layers of GO sheets. In addition, the initial tangent modulus in tension of silicate chain direction can be enhanced by about 38%. Compared to the plain C-S-H, a double-peak phenomenon was identified in the compressive stress-strain response of the intercalated GO/C-S-H composites. This second peak was due to the presence of GO which indicates the increases in the plasticity of the C-S-H gel. The failure of the mode of the intercalated GO/C-S-H was marked by a rapid release of energy with improved fracture energy. The fracture properties were found to be dependent on the initial crack size. The addition of GO increased the fracture energy of the C-S-H gel at notch sizes higher than

15 Å. Based on the pull-out simulation result, the maximum interfacial bond strength was about 0.8 GPa. The proposed MD simulation methodology is a powerful tool for fundamental understanding of the strengthening mechanisms of GO and other nano-additives in cementitious materials at the nanoscale. These insights can be used to design and optimize the macroscale properties of cementitious composites with potential functional features such as self-sensing and self-healing properties.

COMPETING INTERESTS

The authors declare no competing interests.

REFERENCES

[1] K. Sobhan, M. Mashnad, Journal of Materials in Civil Engineering, 14 (2002) 177-184.

[2] M. Ali, A. Majumdar, D. Rayment, Cement and Concrete Research, 2 (1972) 201-212.

[3] W. Sonphuak, N. Rojanarowan, International Journal of Industrial Engineering Computations, 4 (2013) 505-516.

[4] J. Claramunt, M. Ardanuy, J.A. García-Hortal, R.D. Tolêdo Filho, Cement and Concrete Composites, 33 (2011) 586-595.

[5] S. Leonard, A. Bentur, Cement and concrete research, 14 (1984) 717-728.

[6] M.A. Rafiee, J. Rafiee, I. Srivastava, Z. Wang, H. Song, Z.Z. Yu, N. Koratkar, small, 6 (2010) 179-183.

[7] S. Lv, S. Ting, J. Liu, Q. Zhou, CrystEngComm, 16 (2014) 8508-8516.

[8] S. Lv, Y. Ma, C. Qiu, T. Sun, J. Liu, Q. Zhou, Construction and Building Materials, 49 (2013) 121-127.

[9] Z. Pan, L. He, L. Qiu, A.H. Korayem, G. Li, J.W. Zhu, F. Collins, D. Li, W.H. Duan, M.C. Wang, Cement and Concrete Composites, 58 (2015) 140-147.

[10] Q. Zheng, B. Han, X. Cui, X. Yu, J. Ou, Nanomaterials and Nanotechnology, 7 (2017) 1847980417742304.

[11] A.J. Allen, J.J. Thomas, H.M. Jennings, Nature materials, 6 (2007) 311.

[12] R.P. Selvam, V.J. Subramani, S. Murray, K.D. Hall, in, 2009.

[13] I. Richardson, Cement and Concrete Research, 34 (2004) 1733-1777.

[14] R.J.-M. Pellenq, A. Kushima, R. Shahsavari, K.J. Van Vliet, M.J. Buehler, S. Yip, F.-J. Ulm, Proceedings of the National Academy of Sciences, 106 (2009) 16102-16107.

[15] X. Cong, R.J. Kirkpatrick, Advanced Cement Based Materials, 3 (1996) 144-156.

[16] I.G. Richardson, Acta Crystallographica Section B: Structural Science, Crystal Engineering and Materials, 70 (2014) 903-923.

[17] H.M. Jennings, Cement and concrete research, 30 (2000) 101-116.
[18] H.M. Jennings, Cement and Concrete Research, 38 (2008) 275-289.
[19] D. Fan, S. Yang, Construction and Building Materials, 176 (2018) 573-582.
[20] D. Hou, Z. Li, Advances in Cement Research, 27 (2015) 278-288.
[21] R. Shahsavari, R.J.-M. Pellenq, F.-J. Ulm, Physical Chemistry Chemical Physics, 13 (2011) 1002-1011.
[22] W. Wu, A. Al-Ostaz, A.H.-D. Cheng, C.R. Song, Journal of Nanomechanics and Micromechanics, 1 (2011) 84-90.
[23] D. Hou, T. Zhao, P. Wang, Z. Li, J. Zhang, Engineering Fracture Mechanics, 131 (2014) 557-569.
[24] H. Alkhateb, A. Al-Ostaz, A.H.-D. Cheng, X. Li, Journal of Nanomechanics and Micromechanics, 3 (2013) 67-77.
[25] D. Fan, L. Lue, S. Yang, Computational Materials Science, 139 (2017) 56-64.
[26] D. Hou, Z. Lu, X. Li, H. Ma, Z. Li, Carbon, 115 (2017) 188-208.
[27] T. Yang, Y. Jia, D. Hou, H. Li, J. Jiang, J. Zhang, Chemical Physics Letters, 708 (2018) 177-182.
[28] H. Wan, Y. Zhang, Materials and Structures, 53 (2020) 1-12.
[29] L. Lu, Y. Zhang, B. Yin, Computational Materials Science, 173 (2020) 109440.
[30] A. Lerf, H. He, M. Forster, J. Klinowski, The Journal of Physical Chemistry B, 102 (1998) 4477-4482.
[31] K.A. Mkhoyan, A.W. Contryman, J. Silcox, D.A. Stewart, G. Eda, C. Mattevi, S. Miller, M. Chhowalla, Nano letters, 9 (2009) 1058-1063.
[32] J.-A. Yan, M. Chou, Physical review B, 82 (2010) 125403.
[33] R. Lahaye, H. Jeong, C. Park, Y. Lee, Physical Review B, 79 (2009) 125435.
[34] T. Dyer, N. Thamwattana, R. Jalili, RSC Advances, 5 (2015) 77062-77070.
[35] H. Manzano, A.K. Mohamed, R.K. Mishra, P. Bowen, Cement and Concrete Research, 102 (2017) 227-230.
[36] S. Plimpton, Journal of computational physics, 117 (1995) 1-19.
[37] H. Manzano, S. Moeini, F. Marinelli, A.C. Van Duin, F.-J. Ulm, R.J.-M. Pellenq, Journal of the American Chemical Society, 134 (2012) 2208-2215.
[38] D. Hou, T. Zhao, H. Ma, Z. Li, The Journal of Physical Chemistry C, 119 (2015) 1346-1358.
[39] N.V. Medhekar, A. Ramasubramaniam, R.S. Ruoff, V.B. Shenoy, ACS nano, 4 (2010) 2300-2306.
[40] D. Hou, H. Ma, Y. Zhu, Z. Li, Acta materialia, 67 (2014) 81-94.
[41] M.A. Qomi, K. Krakowiak, M. Bauchy, K. Stewart, R. Shahsavari, D. Jagannathan, D. Brommer, A. Baronnet, M. Buehler, S. Yip, Nature communications, 5 (2014) 4960.
[42] W. Zhu, J.J. Hughes, N. Bicanic, C.J. Pearce, Materials characterization, 58 (2007) 1189-1198.

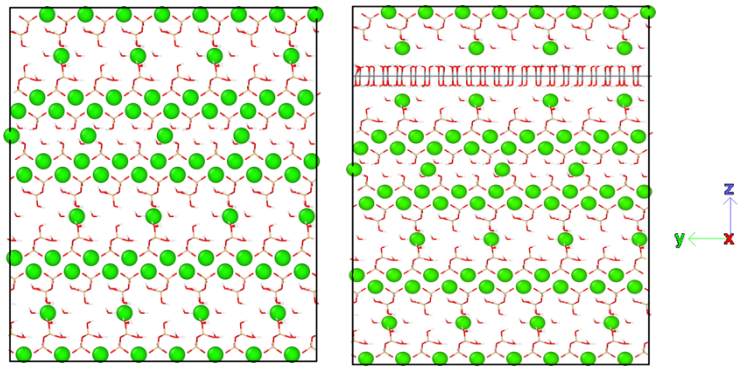

(a) (b)

Figure 1 (a) Molecular structure of C-S-H produced based on Richardson[14] (b) molecular structure of GO/C-S-H compostie structure with one GO sheet (grey atoms are carbon in GO sheet, red atoms are oxygen, white atoms are hydrogen, green atoms are calcium and pearl atoms are silica)

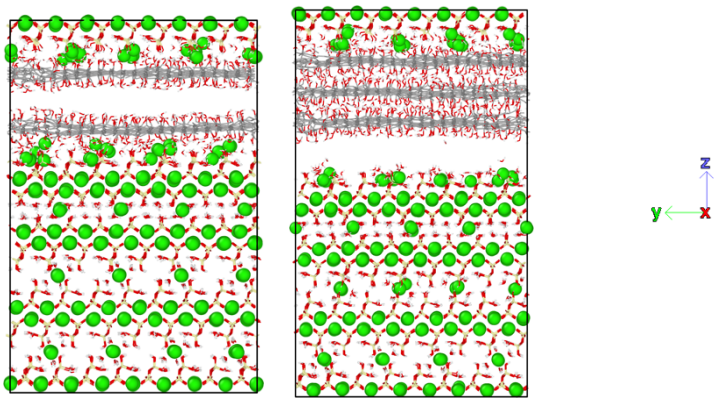

(a) (b)

Figure 2 Molecular structures of GO C-S-H composites with multilayer GO sheets after initial equilibrium (a) two layers of GO sheets (b) three layers of GO sheets

372

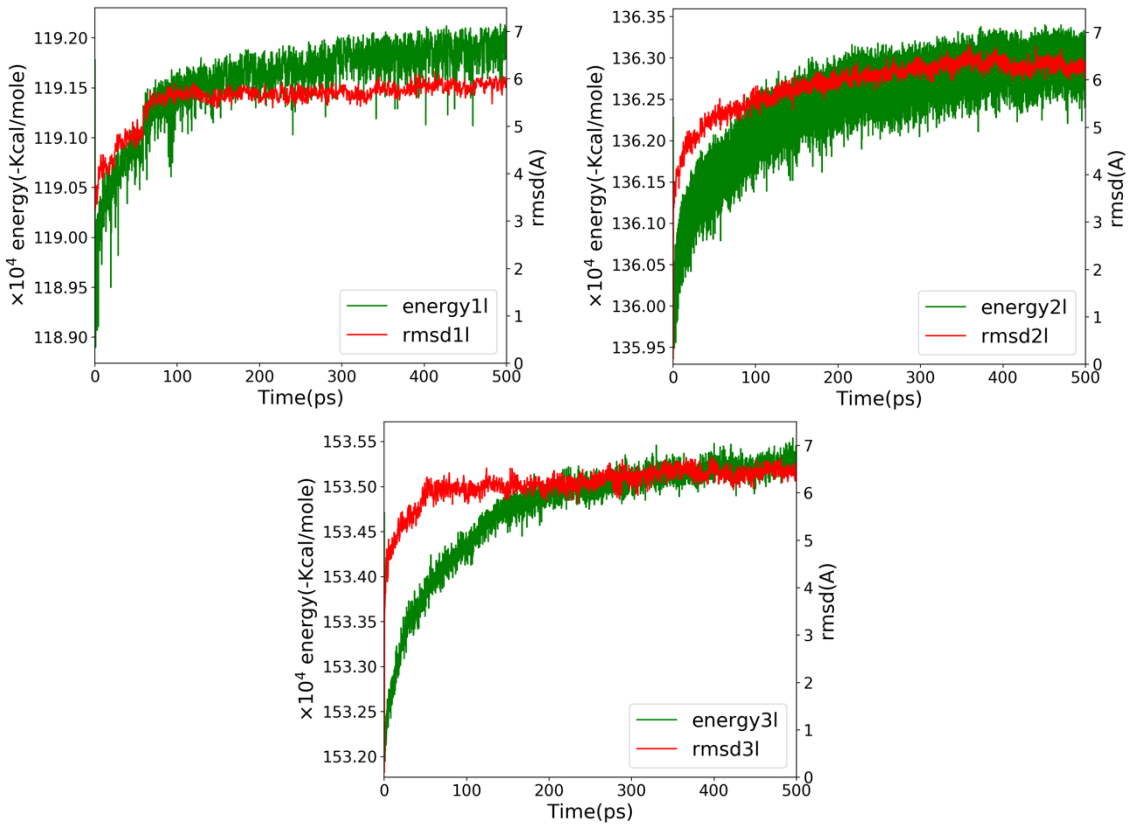

Figure 3 Energy reduction and RMSD value of C-S-H structures with one, two and three layers of GO sheets during energy minimization

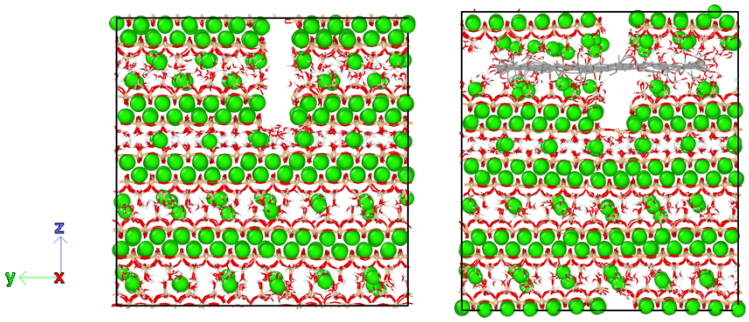

(a) (b)

Figure 4 The structures with a notch depth of 10 Å (a) C-S-H (b) C-S-H with one layer GO sheet

378

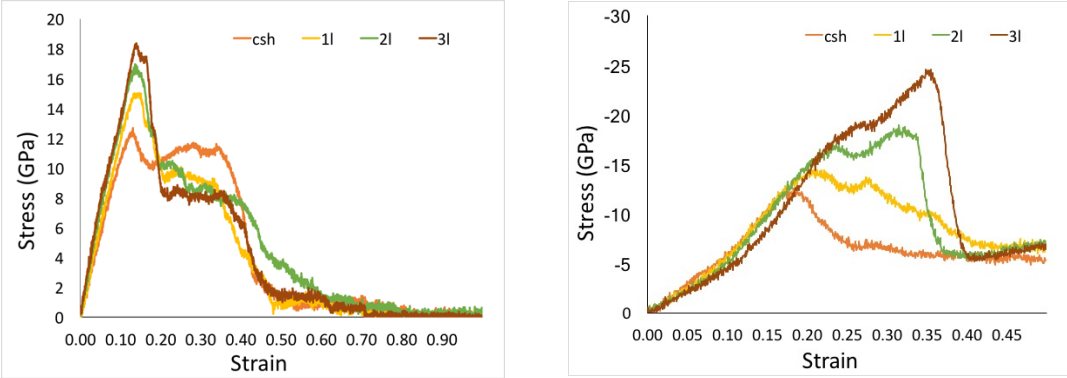

(a) (b)

Figure 5 The stress-strain curves for all GO C-S-H structures (a) under tensile test along y-direction (b) under compression test along z-direction

379

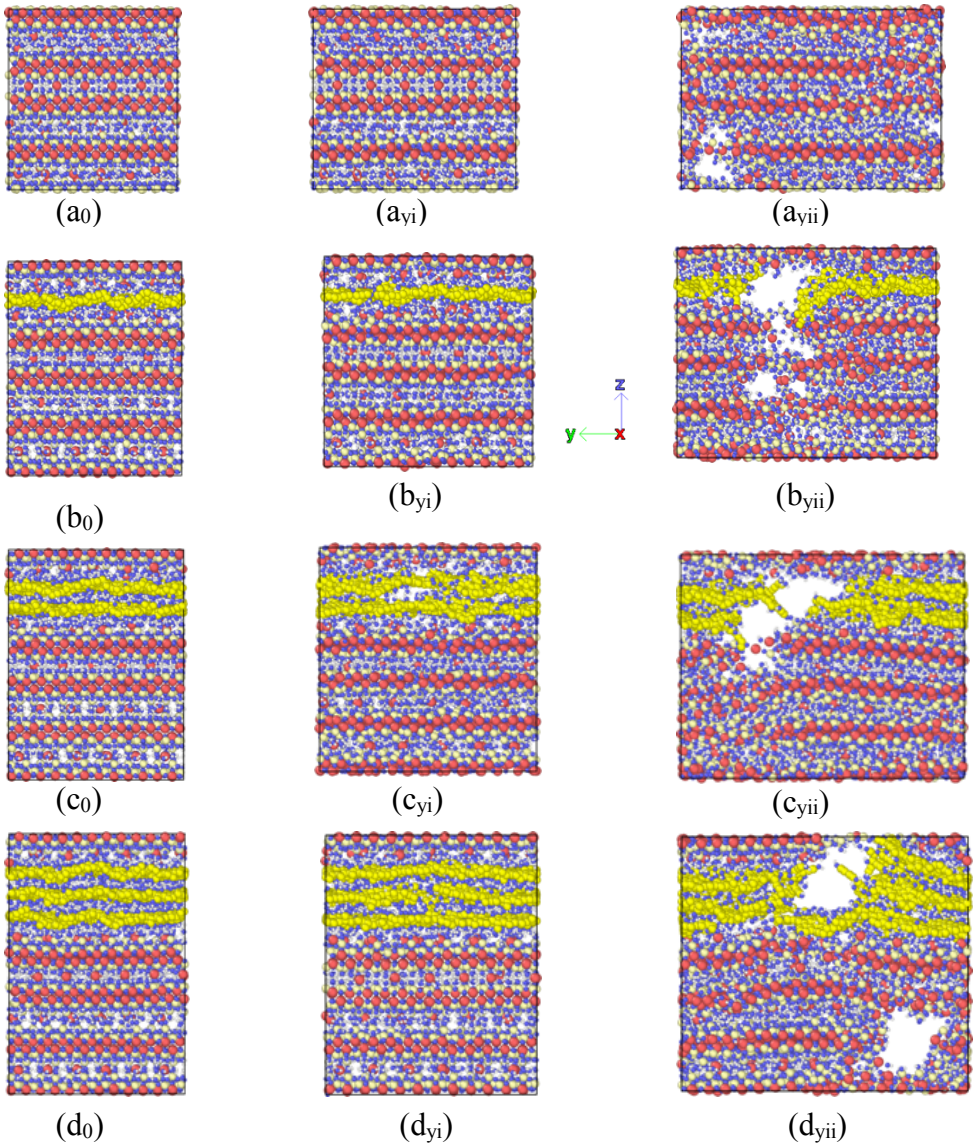

Figure 6 Failure mode of molecular structure of C-S-H and GO/C-S-H composites under tension. (a) C-S-H nanostructure (b) C-S-H with one layer GO sheet (c) C-S-H with two layers GO sheet (d) C-S-H with three layer GO sheet for different loading stages: (0) represents the structure after equilibrium; (i) represents the occasion of the maximum stress, at strain of 0.14; and (ii) represents the occasion after failure happens, at strain of 0.4

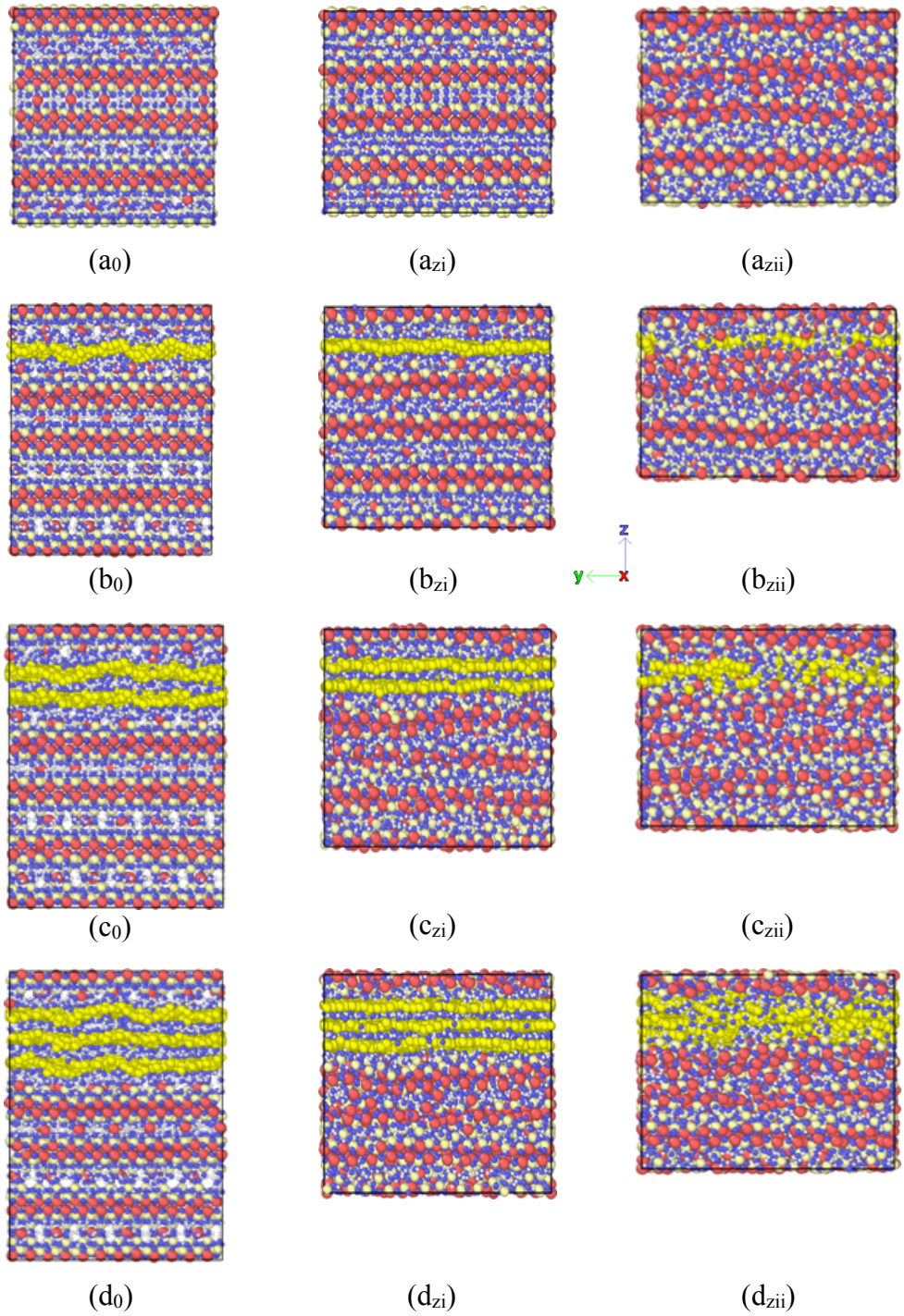

Figure 7 Failure mode of molecular structure of C-S-H and GO/C-S-H composites under compression. (a) C-S-H nanostructure (b) C-S-H with one layer GO sheet (c) C-S-H with two layers GO sheet (d) C-S-H with three layer GO sheet for different loading stages: (0) represents the structure after equilibrium; (i) represents the occasion of the maximum stress; and (ii) represents the occasion after failure happens. The stain of (a_{zi}) is 0.18, (b_{zi}) is 0.21, (c_{zi}) is 0.32 and (d_{zi}) is 0.35; the strain of (a_{zii}) is 0.27 and 0.42 for (b_{zii}), (c_{zii}) and (d_{zii})

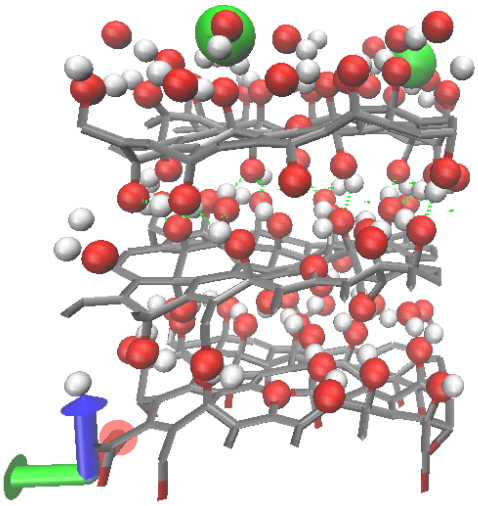

(a)

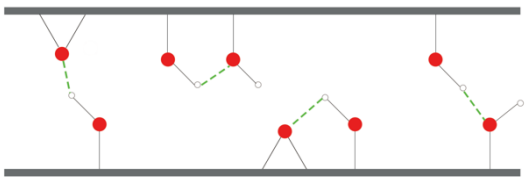

(b)

Figure 8 (a) Atomic structure of partial three GO sheets in the C-S-H interface with hydrogen bonds (b) 2D schematic shows configurations of hydrogen bonds between two GO sheets

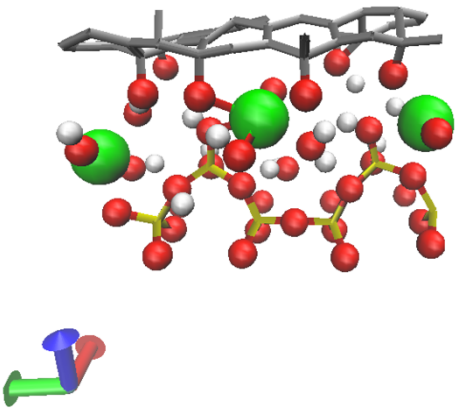

Figure 9 Schematic diagram of partial structure in GO C-S-H nanocomposite. The bonds of one Calcium atom connected with the oxygen atoms in hydroxyl, silica chain and GO sheet are presented

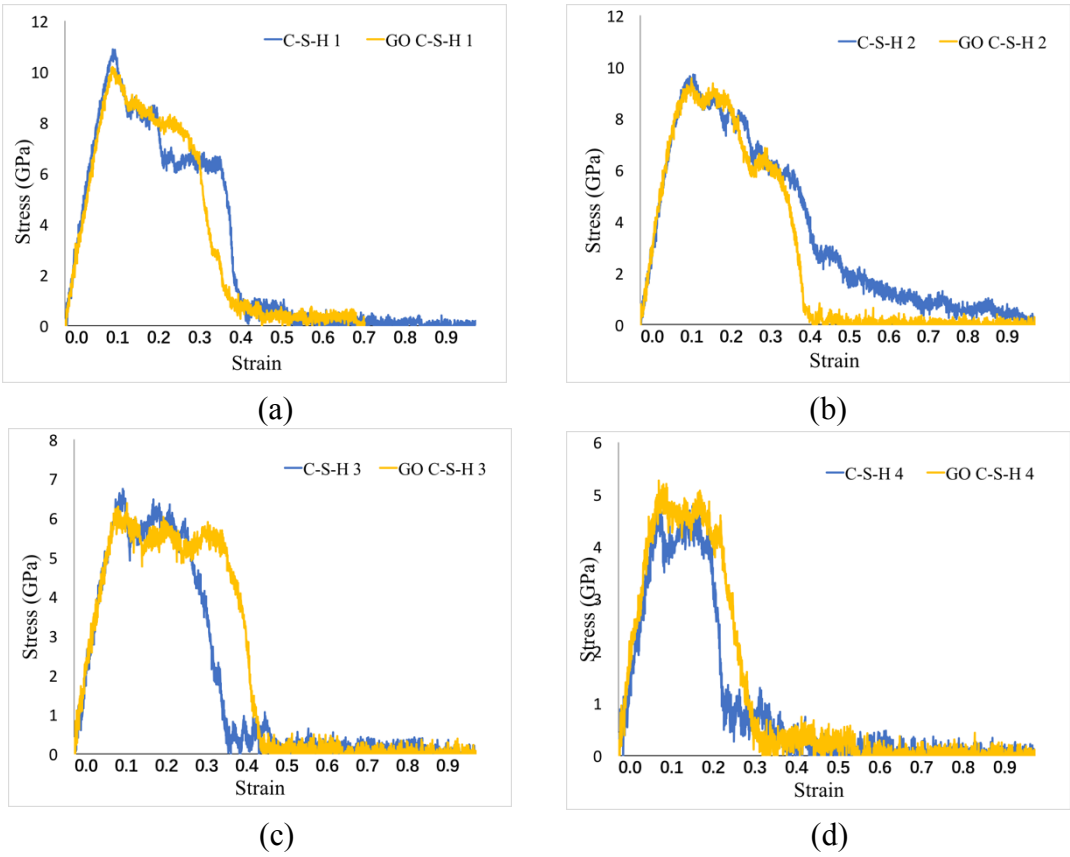

Figure 10 Stress-strain curves of C-S-H structure and one layer GO C-S-H under tension along y-direction with notch in depth of (a) 5 Å (b) 10 Å (c) 15 Å and (d) 20 Å

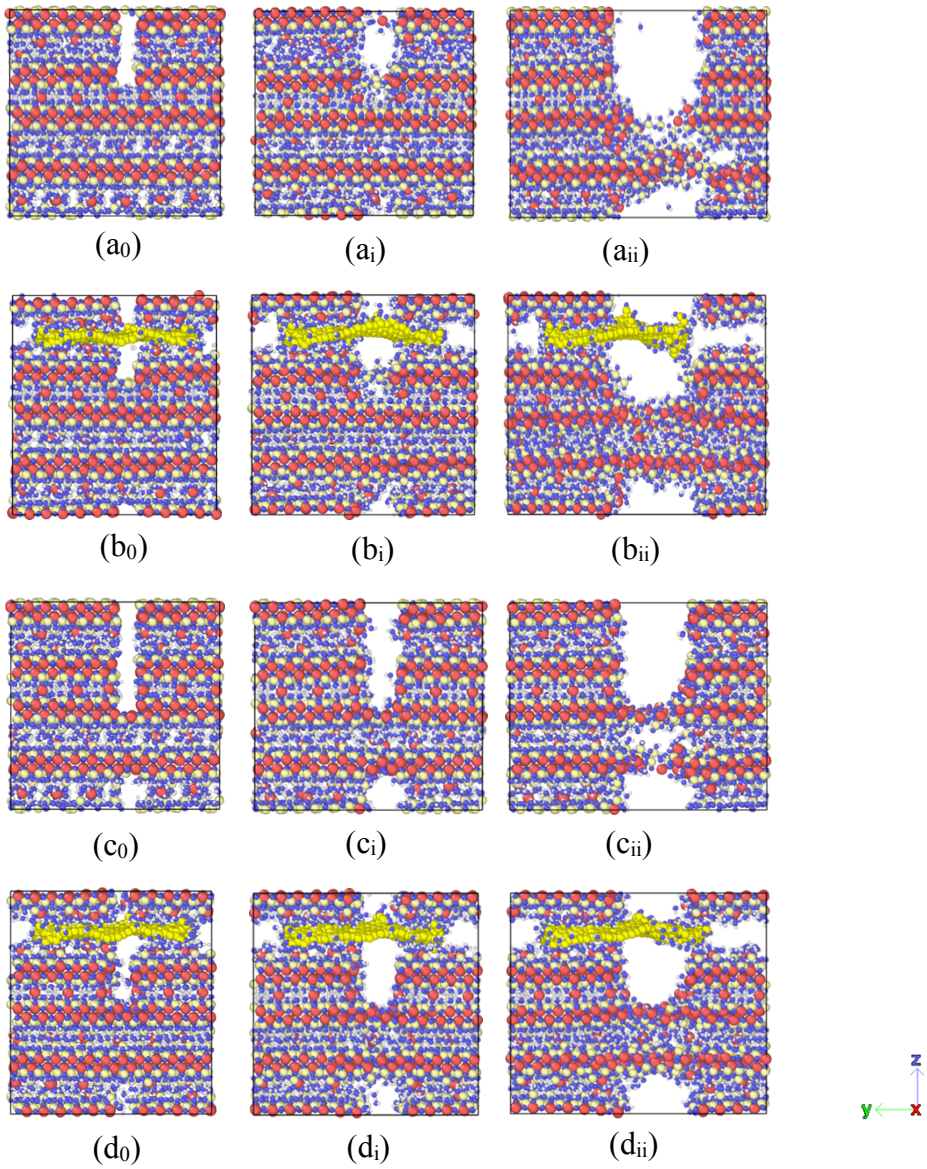

Figure 11 Morphologies under y-direction pulling out for (a) C-S-H nanostructure with a 15Å notch (b) C-S-H inserted with one layer GO sheet in a 15 Å notch (c) C-S-H nanostructure with a 20 Å notch (d) C-S-H inserted with one layer GO sheet in a 20 Å notch under three loading stages, i.e., (0) after equilibrium; (i) the occasion of the maximum stress; and (ii) the occasion when failure happens

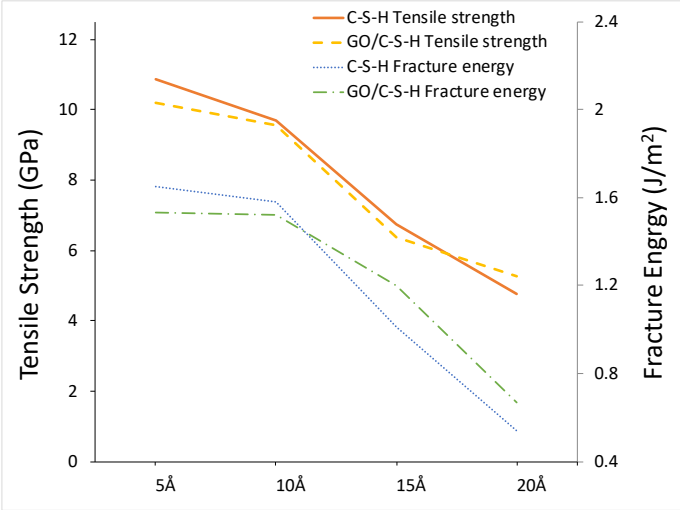

Figure 12 Crack size effect of notch on tensile strength and fracture energy

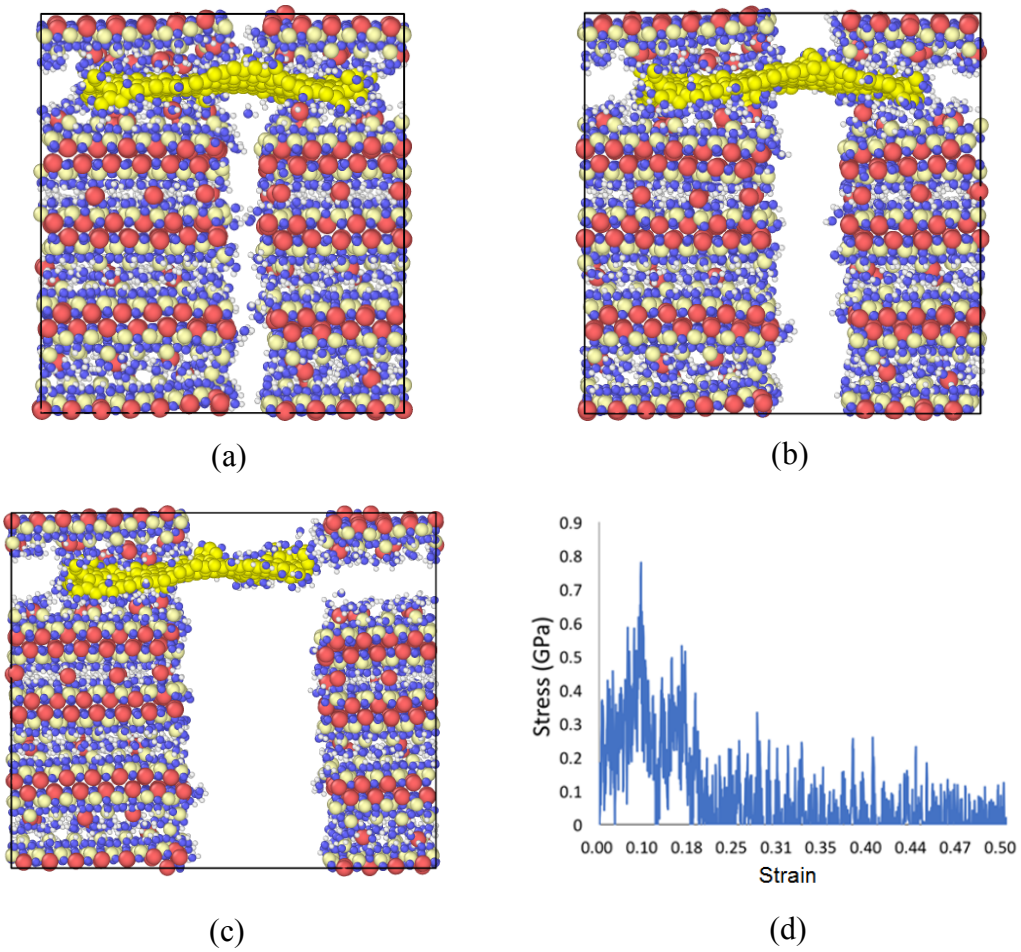

Figure 13 One layer GO sheet enhanced C-S-H nanostructure with an infinite crack under tension (a) at the start; (b) maximum stress happens; (c) de-bonding of GO sheet on one side; and (d) the pull-out stress-strain curve of the GO C-S-H nanostructure